HTML ABSTRACT + LINKS

Microfluidic interfacial tensiometry

Steven D. Hudson, João T. Cabral,[a] William J. Goodrum, Jr.,
Kathryn L. Beers, and Eric J. Amis
Polymers Division, National Institute of Standards and Technology, Gaithersburg, Maryland 20899

(Received 1 February 2005; accepted 5 July 2005; published online 17 August 2005)

A microfluidic approach to measure interfacial tension σ of immiscible fluids rapidly is reported. This method rests upon quantitative real-time analysis of two-phase flow and drop-shape dynamics. Drops of prescribed dimension and spacing are produced, accelerated, and deformed under extensional flow. These measurements compare well with existing published data and demonstrate a wide range of accessible interfacial tension (e.g., from 2.5 to 60 mN/m).
[DOI: 10.1063/1.2034098]

Interfacial tension σ is a central property of immiscible liquids, since it controls their performance as detergents, creams, coatings, reaction media, etc.[1] It is moreover sensitive to impurities and additives, which often migrate to the interface between phases. Interfacial tension is a measure of the work required to increase the interfacial area, normalized to that area, and therefore governs the structure, dynamics and stability of multiphase systems. Consequently, accurate σ measurements are both practically and scientifically relevant.[1,2] Interfacial tension often plays a substantial role in microfluidic devices, typically overwhelming the effects of gravity and inertia, which are often significant at larger dimensions.[3] With these ideas in mind, we develop a microfluidic approach to measuring σ. Our approach uses extensional flow to stretch droplets, is accurate and rapid, uses minimal amounts of reagents (0.01–5 mL), and in certain conditions can be used to probe both static and dynamic surfactant adsorption to the interface.

Our microfluidic tensiometer performs primarily two functions: the formation and deformation of drops. Drop formation occurs at a T junction of two immiscible streams, and drop deformation is induced by flow constrictions along the downstream channel (Fig. 1). Drops may be dispersed under conditions where the capillary number ($\mathrm{Ca}=\eta_c u/\sigma$, where η_c is viscosity of the continuous phase, and u is the flow velocity) is near unity: as demonstrated at either a simple junction of the two fluids[4] or where hydrodynamic focusing is used.[5] However, this condition is undesirable, because the drop formation is sensitive to σ, and it dictates a minimum flow rate. Moreover, if surfactant is present, gradients in interfacial concentration and tension may develop,[6–8] and fluctuations in drop size may be accompanied by variations in surfactant concentration. Under confinement, however, drops (or rather plugs) can be made at very small Ca.[9] At such small Ca, the Marangoni number Ma is large, because it is proportional to the Gibbs-Marangoni elasticity, a constant of order 0.2, and inversely proportional to Ca. As a result, the surfactant layer is incompressible.[10] Since small ($\sim 10\ \mu$m) microfluidic channels can be fabricated, small drops with consistent size and concentration of surfactant can be produced at low flow rate, regardless of interfacial tension.

Whereas confinement is beneficial for drop formation, it complicates drop deformation and relaxation (see later discussion).[11–13] Therefore, wider channels are used to accomplish these functions. When the drops enter this wide channel, however, it is important that their speed be kept relatively constant. In particular, the drops must not slow down to the point of collision, which would force the drops out of position, to different planes of focus, drop speed, and shear rate. Each of these disturbances has detrimental consequences to data analysis. After entering the wider channel, a series of constrictions generate extensional flow gradients that deform the drops modestly as they pass through (Fig. 2), as detailed below.

A custom-built LABVIEW[14] program drives fluid pumps, analyzes images in real time, records drop shape and position, and computes extension rate of the local surrounding fluid. Following Taylor's theory for drop deformation in extensional flow fields,[15] we calculate the material rate of change of the drop deformation D (defined as the difference of major and minor principal radii divided by their sum):

$$\mathrm{D} = (a - b)/(a + b). \tag{1}$$

Experimentally, we compute the deformation from the drop's moments of inertia.

In a converging (or diverging) channel, the flow is accelerating (or decelerating), producing an extensional flow field, which stretches material along (or transverse) to the flow direction and whose rate is equal to the spatial derivative of

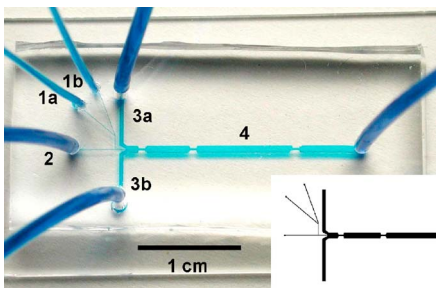

FIG. 1. Image of a device, mounted on a glass slide, fitted with capillaries and filled with liquid dye. During operation, fluid 1 (a and b) is injected as drops into immiscible stream 2. These drops are then fed by 3a and 3b into channel 4 for analysis and measurement. The constrictions in channel 4 accelerate and therefore stretch the drops. Multiple constrictions permit measurement at different interface age. The channel geometry is shown schematically in the inset, at lower right.

[a]Current address: Department of Chemical Engineering, Imperial College London, London SW7 2AZ, UK.

Downloaded 29 Aug 2005 to 129.6.154.48. Redistribution subject to AIP license or copyright, see http://apl.aip.org/apl/copyright.jsp

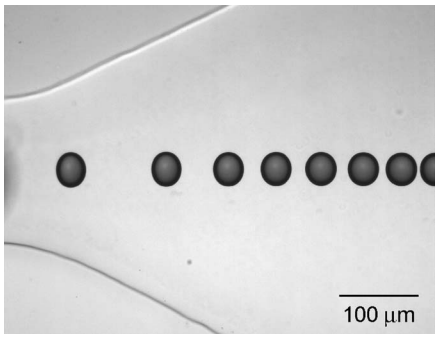

FIG. 2. Freeze-frame image of drops flowing left to right in an extensional flow gradient (water drops in pdms 1000). Measurements can be done at either the entrance or exit of a constriction; the exit is shown here. When the drops leave the constriction (the channel walls appear as slanted lines in the left half of the image), the flow decelerates in proportion to the change in cross-sectional area. The drops, which are generated periodically in time, therefore, become closer together. This deceleration corresponds to a stretching in the transverse direction; note that the drops at the left side are stretched vertically, and their deformation decays as they pass to the right. Here for illustrative purposes the drops are allowed to come relatively close together (which is suboptimal for measurements, because eventually their relaxation is hindered). Generally, the drop production rate is adjusted so that there are a few drops per image.

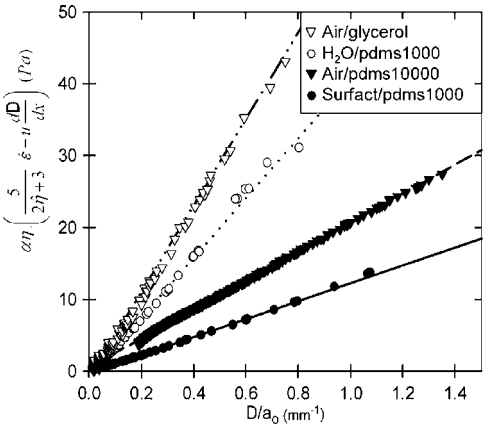

FIG. 3. Experimental analysis of drop deformation upon departure from the channel constriction (Taylor plot): $\alpha\eta_c(5/(2\hat{\eta}+3)\dot{\varepsilon}-u\partial \mathsf{D}/\partial x)$ as a function of D/a_o. The radius a_o, deformation D and trajectory of the drops are measured directly by image analysis, at a rate in excess of 100 data points/s. The slope is equal to the interfacial tension (mN/m).

the velocity. Specifically, for flow along x, the extension rate is written:

$$\dot{\varepsilon} = du/dx = -(dt/dx)^{-2}\, d^2t/dx^2, \tag{2}$$

where t is the time since the drop entered the field of view and u is drop velocity. When drops deform, D depends in general not only on $\dot{\varepsilon}$ but also on drop history. The response $d\mathsf{D}/dt$ is proportional to the difference in D from the steady value of D at the instantaneous value of $\dot{\varepsilon}$:[16]

$$\frac{d\mathsf{D}}{dt^*} = \mathsf{D}_{steady} - \mathsf{D} = \frac{5}{2\hat{\eta}+3}\tau\dot{\varepsilon} - \mathsf{D}, \tag{3}$$

where t^* is the nondimensional time t/τ, and

$$\tau = \frac{(2\hat{\eta}+3)(19\hat{\eta}+16)}{40(\hat{\eta}+1)}\frac{\eta_c a_o}{\sigma} = \frac{\alpha\eta_c a_o}{\sigma} \tag{4}$$

is the characteristic time for drop shape relaxation, a_o is the undistorted drop radius, $\hat{\eta}$ is the relative viscosity of the drop η_d/η_c, and α is a function of $\hat{\eta}$. $d\mathsf{D}/dt$ is the material time derivative of D, which in time-invariant flow is $u\partial\mathsf{D}/\partial x$. To avoid the assumption that the instantaneous deformation approximates D_{steady} (i.e., $d\mathsf{D}/dt \approx 0$),[17] we calculate Eq. (3) directly, i.e., $\alpha\eta_c(5/(2\hat{\eta}+3)\dot{\varepsilon}-u\partial\mathsf{D}/\partial x)$ vs D/a_o (which we name a Taylor plot), so that the slope is σ (Fig. 3).

Although the velocity field in a channel can be computed from its geometry (by solving the Navier–Stokes equation) we are concerned here only with the velocity of the drops themselves. Therefore, our analysis needs neither the detailed geometry nor the entire flow field. Instead, we measure the drop velocity directly, eliminating the need to calibrate each device.

The microfluidic device is fabricated by a rapid prototyping method, using a thiolene frontal photopolymerization (FPP) technique reported earlier[18] or conventional SU8 photolithography. Typical cross section of the deformation channel ranged from 90×700 μm to 850×1250 μm(height h $\times$width w). The width w_c of the constriction is typically $w/3$. Transparent-elastomer (polydimethylsiloxane, PDMS) replicas are treated with low-power oxygen plasma (SP100, Anatech) and then sealed to glass. Finally, the device is heat treated to return the PDMS channels to their hydrophobic condition.

A variety of immiscible fluids were investigated to demonstrate a capability to measure a wide range of interfacial tension (Table I). For each experiment, the temperature was recorded, so that the Arrhenius-adjusted viscosity could be used in data analysis.

Flow was driven by computer controlled syringe pumps (from either New Era or Harvard Apparatus) connected to the microfluidic device. Flow rates were adjusted so that drops were produced at a frequency somewhat less than the camera frame rate and exhibited D exceeding 0.1. Drops are imaged by bright field optical microscopy (Olympus IX71, using either a $4\times$ or $10\times$ objective lens) and appear dark near their edges (Fig. 2). The image acquisition frame rate is 50 Hz, although higher rates have also been used. The exposure time for each image is chosen small enough (e.g., 300 μs) that the motion of drops during this time is less than a full pixel and therefore causes no blurring. Magnification (1.85 or 0.738 μm/pixel, respectively) is calibrated using a diffraction grating. Typical image size is 240×1000 pixels.

The images are analyzed in real time (i.e., at a frequency equal to the camera frame rate) to obtain the position, deformation and radius of the drops as they pass through the image window. Since each frame usually contains a few drops, this system collects more than 100 data points each second. Periodically (e.g., every 2 s), drop transit time $t(x)$ and deformation are fit to polynomials (the results are insensitive to polynomial order ranging from 5 to 7) to compute $\partial\mathsf{D}/\partial x$ and $du/dx=\dot{\varepsilon}$. At the same time, $\alpha\eta_c(5/(2\hat{\eta}+3)\dot{\varepsilon}-u\partial\mathsf{D}/\partial x)$ is fit to a linear function of D/a_o (Fig. 3), to yield σ.

Measurements of σ ranging from 2.5 to ~60 mN/m have been demonstrated (Table I). Smaller values of σ can always be studied by decreasing the flow rate. On the other hand, the maximum measurable value of σ is proportional to the camera frame rate, viscosity, and a_o [Eq. (4)] and roughly proportional to $1n(w/w_c)$, where w/w_c is the contraction ratio of the channel constriction [which influences $\dot{\varepsilon}$, Eq. (3)]. Design tradeoffs for various measurement goals are possible. Here, use of a considerable range of viscosity and relative drop viscosity is reported. Although the measured values of σ are insensitive to drop size a_o, its control is important, as it

Downloaded 29 Aug 2005 to 129.6.154.48. Redistribution subject to AIP license or copyright, see http://apl.aip.org/apl/copyright.jsp

TABLE I. Summary of interfacial tension results (and fluid viscosities).[a]

Interface	σ(mN/m)	σ_{lit}
Ppms500/pdms1000[b]	2.52±0.27	
Surfactant solution[c]/pdms1000	12.7±0.4	
Ethyleneglycol/pdms1000	17.6±0.7	
Air/pdms1000	23.8±1.0	21.2[23]
	25.0±0.8; 25.1±1.2	
Air/pdms10000	22.9±1.5; 22.6±2.1; 21.9±0.8; 20.8±1.5	21.5[23]
H_2O/pdms1000	41.2±1.1; 41.5±1.6	41.4[24]
	41.0±2.8; 41.7±3.0	
H_2O/pdms10000	39.2±3.4	41.4[24]
Air/ppms500	24.2±1.3	28.5[23]
Glycerol/ppms500	21.2±3.0; 20.4±2.5	
Air/glycerol	59.8±2.5; 58.5±2.7	59.2[25]
Fluid	η(Pa s) (@ 22 °C)	
Air	0.00002	
H_2O	0.001	
Ethyleneglycol	0.02[26]	
Glycerol	0.925[26]	
Poly(phenylmethylsiloxane) (ppms500)	0.637[23]	
Poly(dimethylsiloxane) (pdms1000)	1.02[23]	
Poly(dimethylsiloxane) (pdms10000)	10.3[23]	

[a]The uncertainty is the standard deviation of individual measurements (15–200) of σ. Multiple values are reported for measurements repeated at different flow rate or at different room temperature (ranging from 21.2 to 22.8 °C). Literature sources of measurements at 25 °C are cited. (The interfacial tension of these pure systems, with negligible mutual solubility, depends only very weakly on temperature.)
[b]For the silicone fluids, identification numbers in the left column are approximate kinematic viscosity (cSt). Literature sources are cited.
[c]2% mass $EO_{19}PO_{30}EO_{19}$ in water.

sets the drop relaxation rate. In these experiments, a_o has been adjusted from 9 to 220 μm (using channels of different cross section). As such, a_o is typically less than $h/4$. Within experimental uncertainty, the measured value of σ is independent of drop size, even though the analysis assumes unbounded flow. Further work will explore the effects of boundaries, which affect drop velocity and deformation, when the drop size becomes similar to the channel dimensions.[11,12,19–21] These effects are least significant when $\hat{\eta} \ll 1$. Data in this regime indicate that these effects do not affect the measurement of σ significantly until the drop diameter is nearly as large as h.

These measurements have accuracy and precision of approximately several percent (Table I). The main source of error seems to be in determining the function $t(x)$, from which $\dot{\varepsilon}$ derives [Eq. (2)]. Accuracy relies upon stability of flow rate and drop position relative to the centerline. Measurements were carried out at both the entrance and the exit of channel constrictions, and these results are consistent when the drop velocity and the maximum deformation are moderate (e.g., 400 pixels/s and 0.1, respectively).

Not only does this tensiometer function with unprecedented rapidity and low reagent consumption, its microfluidic approach has inherent features that are attractive. Flow through the channel produces a direct and simple relationship between the position along the channel and the age of the interface, an important parameter for some surfactant systems. For this reason, multiple constriction points are placed in the channel. In addition to the adsorption of surfactant, the kinetics of competitive adsorption from the carrier fluid can also be explored, if additional inputs are introduced downstream. Surfactant solutions may be sensitive to flow rate, because flow can cause depletion of surfactant on the interface and can produce interfacial concentration gradients.[8] When such gradients are significant, it is useful to examine the entire drop surface rather than simply its moments.[22] For the simple fluid compositions reported here, the tension is invariant to interface age (0.3–25 s) and flow rate, within experimental uncertainty.

In summary, we demonstrate a microfluidic strategy to measure interfacial tension between immiscible fluids. We employ soft lithography, optical microscopy, and real-time image analysis to produce and interrogate micron-sized drop dynamics. This approach is suitable to the study of interfacial dynamics of complex systems with rapidity, small reagent consumption and accuracy.

The support of ICI/National Starch, Procter and Gamble, the National Institute of Standards and Technology (NIST) Materials Science and Engineering Laboratories Directors Reserve, and the NIST Combinatorial Methods Center (www.nist.gov/combi) is gratefully acknowledged.

[1] A. W. Adamson and A. P. Gast, *Physical Chemistry of Surfaces*, 6th ed. (Wiley, New York, 1997).
[2] *Drops and Bubbles in Interfacial Research*, edited by D. Mobius and R. Miller (Elsevier, New York 1998).
[3] H. A. Stone, A. D. Stroock, and A. Ajdari, Annu. Rev. Fluid Mech. **36**, 381 (2004).
[4] T. Thorsen, R. W. Roberts, F. H. Arnold, and S. R. Quake, Phys. Rev. Lett. **86**, 4163 (2001).
[5] S. L. Anna, N. Bontoux, and H. A. Stone, Appl. Phys. Lett. **82**, 364 (2003).
[6] R. A. deBruijn, Chem. Eng. Sci. **48**, 277 (1993).
[7] C. D. Eggleton, T. M. Tsai, and K. J. Stebe, Phys. Rev. Lett. **87**, 048302 (2001).
[8] C. D. Eggleton and K. J. Stebe, J. Colloid Interface Sci. **208**, 68 (1998).
[9] J. D. Tice, H. Song, A. D. Lyon, and R. F. Ismagilov, Langmuir **19**, 9127 (2003).
[10] J. Blawzdziewicz, E. Wajnryb, and M. Loewenberg, J. Fluid Mech. **395**, 29 (1999).
[11] T. Mikami and S. G. Mason, Can. J. Chem. Eng. **53**, 372 (1975).
[12] J. G. Hagedorn, N. S. Martys, and J. F. Douglas, Phys. Rev. E **69**, 056312 (2004).
[13] Y. Son and K. B. Migler, Polymer **43**, 3001 (2002).
[14] Certain commercial materials and equipment are identified in this letter in order to adequately specify the experimental procedure. In no case does such identification imply recommendation or endorsement by the National Institute of Standards and Technology, nor does it imply that these are necessarily the best available for the purpose.
[15] G. I. Taylor, Proc. R. Soc. London, Ser. A **146**, 501 (1934).
[16] J. M. Rallison, Annu. Rev. Fluid Mech. **16**, 45 (1984).
[17] C. Testa, I. Sigillo, and N. Grizzuti, Polymer **42**, 5651 (2001).
[18] J. T. Cabral, S. D. Hudson, C. Harrison, and J. F. Douglas, Langmuir **20**, 10020 (2004).
[19] G. Hetsronni, S. Haber, and E. Wacholder, J. Fluid Mech. **41**, 689 (1970).
[20] B. P. Ho and L. G. Leal, J. Fluid Mech. **71**, 361 (1975).
[21] W. L. Olbricht and L. G. Leal, J. Fluid Mech. **115**, 187 (1982).
[22] Y. T. Hu and A. Lips, Phys. Rev. Lett. **91**, 044501 (2003).
[23] Gelest Silicone Fluids, engineering and design properties. http://www.gelest.com/company/pdfs/siliconefluids.pdf (2004).
[24] T. Svitova *et al.*, Langmuir **18**, 6821 (2002).
[25] Ch. Wohlfarth and B. Wohlfarth, *Surface Tension of Pure Liquids and Binary Liquid Mixtures* (Springer, Berlin, 1997).
[26] C. L. Yaws, *Handbook of Transport Propety Data: Viscosity, Thermal Conductivity, and Diffusion Coefficients of Liquids and Gases* (Gulf, Houston, 1995).

Downloaded 29 Aug 2005 to 129.6.154.48. Redistribution subject to AIP license or copyright, see http://apl.aip.org/apl/copyright.jsp